applied mechanics

MDPI

Article

Biotribological Wear Prediction of Alumina–Polymer Hip Prostheses Using Finite Element Analysis

Mhd Ayham Darwich [1], Hasan Mhd Nazha [2,*], Hiba Mohsen Ghadir [3] and Ahmad Salamah [3]

[1] Department of Bioinformatics, Faculty of Biomedical Engineering, Al-Andalus University for Medical Sciences, Tartous P.O. Box 101, Syria; a.darwich@au.edu.sy
[2] Institute of Mechanics, Faculty of Mechanical Engineering, Otto Von Guericke University Magdeburg, Universitätsplatz 2, 39106 Magdeburg, Germany
[3] Department of Design and Production Engineering, Faculty of Mechanical and Electrical Engineering, University of Latakia, Latakia P.O. Box 101, Syria; hiba.m.ghadir@tishreen.edu.sy (H.M.G.); ahmadsalamah@tishreen.edu.sy (A.S.)
* Correspondence: hasan.nazha@ovgu.de

Abstract

This study investigates the biotribological performance of alumina–UHMWPE and alumina–PEEK hip implant couples through finite element simulation (ANSYS v24) and statistical inference (STATA v17). During gait cycle loading simulations, significant disparity in wear behaviour was observed. Alumina–UHMWPE demonstrated superior mechanical resistance, with a wear volume of 0.18481 mm^3 and a wear depth of 6.93×10^{-4} mm compared to alumina–PEEK, which registered higher wear (volume: 8.4006 mm^3; depth: 3.15×10^{-2} mm). Wear distribution analysis indicated alumina–UHMWPE showed an even wear pattern in comparison to the poor, uneven alumina-PEEK high-wear patterns. Statistical comparison validated these findings, wherein alumina–UHMWPE achieved a 27.60 hip joint wear index (HCI) value, which is better than that of alumina–PEEK (35.85 HCI), particularly regarding key parameters like wear depth and volume. This computational–statistical model yields a baseline design for biomaterial choice, demonstrating the potential clinical superiority of alumina–UHMWPE in reducing implant failure risk. While this is a simulation study lacking experimental validation, the results pave the way for experimental and clinical studies for further verification and refinement. The approach enables hip arthroplasty design optimization with maximal efficiency and minimal resource-intensive testing.

Keywords: hip joint protheses; finite element method; biotribology; frictional wear

Received: 11 May 2025
Revised: 12 June 2025
Accepted: 13 June 2025
Published: 24 June 2025

Citation: Darwich, M.A.; Nazha, H.M.; Ghadir, H.M.; Salamah, A. Biotribological Wear Prediction of Alumina–Polymer Hip Prostheses Using Finite Element Analysis. *Appl. Mech.* **2025**, *6*, 46. https://doi.org/10.3390/applmech6030046

1. Introduction

The hip joint represents one of the most biomechanically critical articulations in the human musculoskeletal system, serving as the vital connection between the femoral head and acetabulum while supporting dynamic weight-bearing functions [1,2]. Progressive degeneration from conditions like osteoarthritis, avascular necrosis, and inflammatory arthritis frequently compromises joint integrity, often necessitating total hip replacement (THR) to restore mobility and alleviate chronic pain [3–5]. With over 350,000 THR procedures performed annually in the United States alone, this intervention has become a cornerstone of orthopaedic surgery, yet long-term implant durability remains challenged by wear-induced osteolysis and aseptic loosening [6,7].

Biotribological performance constitutes a fundamental determinant of prosthetic longevity, where material selection critically influences wear resistance and clinical outcomes [8]. Conventional bearing surfaces predominantly utilize metal-on-polymer (M-o-P) and ceramic-on-polymer (C-o-P) configurations, with ultra-high-molecular-weight polyethylene (UHMWPE) establishing itself as the gold-standard polymeric component due to its favourable biocompatibility and tribological properties [9,10]. However, the generation of UHMWPE wear debris and associated inflammatory responses continue to drive research into alternative bearing materials [11]. Polyetheretherketone (PEEK) has emerged as a promising candidate, offering unique advantages, including a modulus approximating cortical bone to mitigate stress-shielding effects, alongside inherent chemical stability [12,13]. While preliminary studies suggest PEEK's potential in arthroplasty applications, comprehensive evaluations of its long-term wear performance relative to UHMWPE remain limited, particularly under physiologically relevant loading conditions [14,15].

This study addresses this critical knowledge gap through the development of an integrated computational–statistical framework combining finite element analysis (FEA) and quantitative performance metrics to systematically evaluate alumina–UHMWPE and alumina–PEEK bearing couples. Building upon recent clinical wear analyses by Pierce et al. [15] and fundamental tribological studies by Smith and Jones [16] and Khan et al. [17], our study introduces three key innovations: (1) the implementation of dynamic gait cycle loading to simulate physiological wear patterns, (2) the development of the Hip Corrosion Index (HCI) as a novel multi-parameter wear assessment metric, and (3) a comparative statistical analysis of wear distribution characteristics between material pairs.

By bridging computational modelling with clinical wear assessment methodologies, this work provides critical insights for evidence-based biomaterial selection in prosthetic design while establishing a framework for future experimental validation studies.

- Wear Mechanisms and Influencing Factors

The complexity of wear processes arises from the interplay of multiple factors, among which surface roughness, lubrication conditions, and sliding distance are paramount. Surface roughness governs initial contact mechanics and debris formation, while lubrication regimes—ranging from boundary to hydrodynamic—directly modulate friction and wear modes. Sliding distance, as a cumulative measure of interaction, determines long-term wear volume and energy dissipation. Recent investigations underscore that omitting these factors in predictive models can lead to significant underestimation of material degradation, particularly in applications involving cyclic loading or heterogeneous materials. To address this, our analysis explicitly incorporates these parameters, aligning with contemporary frameworks that emphasize multi-factor wear analysis.

- Challenges in Wear Prediction

Despite their widespread use, conventional wear prediction methods face inherent limitations. Experimental approaches, while empirically grounded, often entail prohibitive costs and time investments, especially when replicating multifactorial operational conditions. Moreover, in vitro simulations struggle to capture the dynamic complexities of in vivo environments, such as evolving lubricant chemistry or biological interactions, which are critical for applications like biomedical implants. Analytical models, though computationally efficient, frequently oversimplify contact mechanics by neglecting localized phenomena like micro-scale abrasion or third-body particle effects. These constraints highlight the need for complementary approaches capable of bridging the gap between controlled experimentation and real-world operational scenarios.

- Rationale for FEM Implementation

The selection of Finite Element Modelling (FEM) for this study is rooted in its capacity to overcome several limitations inherent to traditional wear prediction methods. By simulating transient contact stresses and subsurface deformation, FEM offers a nuanced understanding of wear mechanisms that experimental setups may miss due to cost or practicality constraints. This approach is particularly advantageous for scenarios involving complex geometries, multi-axial loading, or material heterogeneities, where empirical testing becomes impractical. While FEM cannot fully supplant long-term experimental validation, it provides a robust platform for preliminary analysis and mechanistic insight, reducing reliance on iterative physical trials. Nevertheless, the fidelity of FEM results hinges on rigorous calibration against empirical wear metrics—such as scar morphology or mass loss—to mitigate simplifications inherent in material modelling assumptions.

2. Basic Components of the Human Hip

The hip joint is the significant joint between the lower limbs and the trunk, formed by the articulation of the femur (thigh bone) with the pelvis. A synovial ball-and-socket joint functionally, it both supports the body's weight and permits movement of the upper leg. Among the body's weight-bearing joints, the hip is second only to the knee in the mechanical stresses it sustains [18].

Anatomically, the hip joint consists of several interconnected structures that work together. The bony framework includes the spherical femoral head and the cup-shaped acetabulum of the pelvis. These are surrounded by fibrocartilaginous structures like the acetabular labrum, with cartilage protective layers covering the articulating surfaces. Stability is provided by the capsular ligaments, and the synovial membrane is responsible for lubrication (Figure 1). The joint movement is powered by surrounding muscles and tendons, with synovial bursae reducing friction during motion. Completing the complex structure are the neurovascular structures that supply essential nutrients and neural control [19].

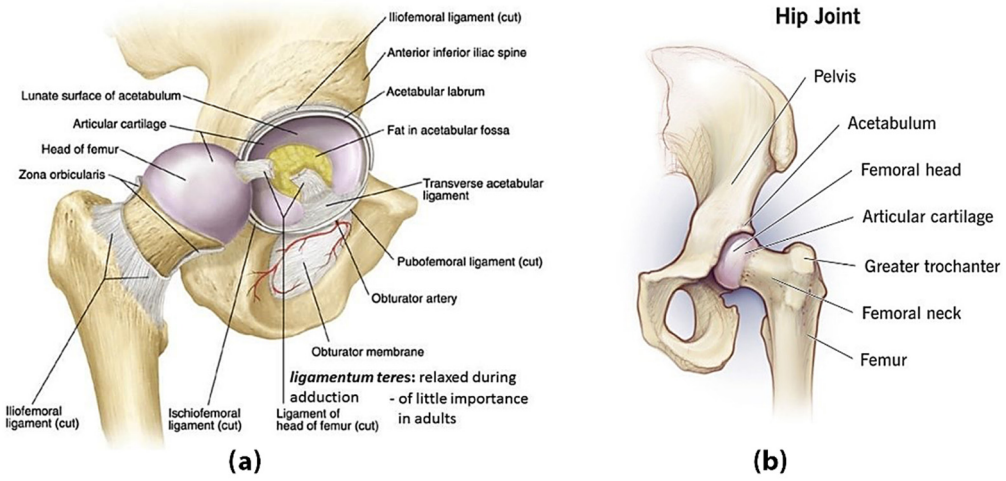

Figure 1. Overall structure of hip joint. (**a**) Schematic showing anatomical components of the human hip joint including femoral head, acetabulum, ligaments, and cartilage; (**b**) medical illustration of the joint in situ, emphasizing its load-bearing and rotational functions.

The femur head, a ball-like protrusion at the top of the femur, is well adapted to the acetabular socket of the pelvis to form a stable yet movable joint [20]. This type of arrangement enables a large variety of movements, including flexion and extension (forward and backward movement), abduction and adduction (sideways movement), and medial and lateral rotation (inward and outward rotation of the thigh) [21].

3. Hip Joint Replacement

Hip arthroplasty, or hip replacement surgery, is a surgical medical intervention wherein an orthopaedic surgeon excises the deformed portions of the human hip joint and replaces them with a prosthetic implant (Figure 2). The artificial hip joint performs the same function as the natural hip joint. This operation has been the most suitable option to relieve pain from a damaged or diseased hip joint and to improve the function in patients with advanced hip conditions such as osteoarthritis, rheumatoid arthritis, avascular necrosis, septic arthritis, or hip fractures that cannot be repaired and improve mobility [21,22]. The early experiments in hip replacement were undertaken in Germany by Gluck in 1890, with replacement of the head of the femur with ivory [3]. The first-ever total hip replacement was performed in 1938. Wiles performed a stainless-steel implant for the femur and the acetabulum, which performed magnificently well in the short term. Designs that evolved from Wiles' designs were not successful, with loss of fixation resulting in failure rates as high as 50%. The technique used in joint replacements today has evolved from Sir John Charnley's work in the 1970s. His design included three parts: a stainless-steel femoral part, which was initially built from stainless steel; an ultra-high-molecular-weight polyethylene acetabular part; and bone cement, using synovial fluid to lubricate the prosthetic joint, creating a decrease in friction [3]. There are two types of hip replacement: total hip replacement (THR), or total hip arthroplasty (THA), which entails the removal of both the damaged femoral head (the ball) and the acetabular cup (the socket) and their replacement with man-made components; and hemi replacement (hemiarthroplasty), entails the replacement of the head of femoral alone, and an artificial one is implanted [23].

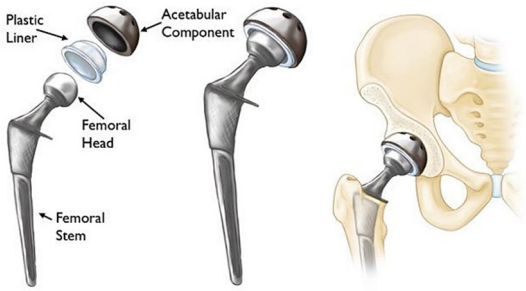

Figure 2. Types of hip replacement (total hip replacement and hemi replacement). Visual representation of the two major types of hip arthroplasty. Total hip replacement (THR) involves replacement of both the femoral head and acetabular socket; hemiarthroplasty replaces only the femoral head, retaining the natural acetabulum.

4. Materials and Methods

Two combinations were chosen to compare the evaluation of wear mechanisms in the artificial hip joint, alumina–UHMWPE and alumina–PEEK, based on their distinct material properties, clinical relevance, and potential impact on implant life.

First: Metal Materials:

- Titanium–Aluminium–Vanadium Alloys (Ti-6A1-4V):

This is an alfa beta titanium alloy exhibiting high energy and favourable erosion resistance. Furthermore, it is used in biomedicine. It has a chemical composition of nearly 90% titanium, 6% aluminium, 4% vanadium, 0.25% (max.) iron, and 0.2% (max.) oxygen. It has high energy, a low elasticity factor, is easy to weld, and is responsive to treatment by heat. It is the most widely used of all the titanium alloys and is utilized in a wide range of diverse applications where low density and exceptional corrosion resistance are required, such as in aerospace and biomechanical applications (implants and prosthetics).

Second: Ceramic Materials:

- Alumina (AL_2O_3):

Aluminium oxide (Al_2O_3) or alumina is one of the most used ceramics in orthopaedics for hip implants. It has various applications in engineering and biomedical fields. Some common examples include bio-ceramics and orthopaedic and dental implants. Due to its thermal, mechanical, and tribological properties (having very high hardness, low friction and excellent wear, corrosion resistance, and chemical stability), alumina is possible to use for orthopaedic applications of articulating surfaces. To achieve the long-term stability of alumina for orthopaedic applications, the material must be free from porosity, and its microstructure must be fine and homogeneous [24,25].

- Zirconia (ZrO_2):

The term "zirconium" is taken from the Arabic name Zargon, meaning "golden coloured," from the Persian words Zar (gold) and Gun (colour) [26]. Zirconia ceramics have been used in the manufacture of femoral heads for total hip replacements due to their superior strength-to-weight ratio and fracture resistance.

Zirconia is polymorphic, which crystallizes in three phases: monoclinic (M), tetragonal (T), and cubic (C). Pure zirconia exists in the monoclinic form at room temperature, being stable up to 1170 °C. At temperatures above this, it is converted to the tetragonal phase, ultimately converting into the cubic structure at 2370 °C [24–26].

Third: Polymeric Materials:

- Polyethylene (Ultra-High-Molecular-Weight Polyethylene) (UHMWPE):

Ultra-high-molecular-weight polyethylene (UHMWPE) is a thermoplastic. It is used in biomedical applications due to its high wear resistance, ductility, and biocompatibility. Much research in recent decades has focused on further improving its mechanical and tribological performances to provide durable implants for patients. It has long chains. The longest chain tends to transfer the load in a more effective way toward the backbone of the polymer by enhancing the activities among molecules [27].

- Polyetheretherketone (PEEK)

Polyetheretherketone, PEEK, is a semi-crystalline thermoplastic polymer that has an aromatic molecular backbone characterized by the repeating chemical formula (–C6H4–O–C6H4–O–C6H4–CO–)n [20]. PEEK, which is an engineering polymer, has gained significant interest in the biomedical field since it has an unorthodox set of mechanical and thermal properties. The material displays excellent heat resistance and chemical stability along with structural integrity when subjected to mechanical loading, which renders it most suitable for medical implants [28].

Interestingly, PEEK possesses an elasticity modulus that is comparable to that of human bone tissue, which is responsible for reducing stress-shielding effects in orthopaedic applications. Its excellent biocompatibility and compatibility with bioactive materials have found widespread application in dental implants and prosthetic parts [28]. The superior strength-to-weight ratio of the polymer has enabled its application in challenging orthopaedic applications, including femoral components and total hip replacement systems [29]. These mechanical properties are quantitatively presented in Table 1.

Table 1. Mechanical properties of the TI-6AL-4V, alumina (AL_2O_3), zirconia, UHMWPE, and PEEK materials.

Material Properties	AL_2O_3	Ti-6Al-4V	UHMWPE	PEEK
Density (kg/m^3)	3980	4500	936	1300
Poisson's ratio	0.23	0.32	0.46	0.3

Table 1. *Cont.*

Material Properties	AL_2O_3	Ti-6Al-4V	UHMWPE	PEEK
Young's modulus (GPa)	370	110	0.5–0.8	3.6
Yield strength (MPa)	15.4	900	17	100
Ultimate strength tensile (MPa)	240	900	39–48	139

4.1. Selecting Materials for Each Element of the Components of Artificial Joints

An artificial hip joint consists of four parts:

1. Acetabular cup component: Ti-6Al-4V.
2. Insert component: Two types of materials were chosen for comparison: UHMWPE and PEEK.
3. Femoral head component: Alumina (AL_2O_3).
4. Stem Component: Ti-6Al-4V.

- ❖ Alumina–UHMWPE: This combination has long been proven effective in total hip replacement (THA) surgery due to its excellent hardness, wear resistance, and biocompatibility. Further, ultra-high-molecular-weight polyethylene (UHMWPE) is a traditional bearing surface. The alumina ceramic femoral head reduces the wear of the polyethylene, reducing osteolysis and aseptic loosening risks. However, concerns remain regarding the fragility and potential for the fracturing of alumina, necessitating continued comparisons [30–33].
- ❖ Alumina–PEEK: Polyether ether ketone (PEEK) is a high-performance thermoplastic material with good mechanical properties, an elastic modulus similar to that of cortical bone, and excellent chemical stability. When combined with alumina ceramics, PEEK may offer advantages such as reduced stress shielding, and potentially different wear behaviour compared to UHMWPE [31–35].

Clinical questions addressed in these comparisons:

- Wear rate and debris generation: How do wear debris size and particle shape differ between alumina–UHMWPE and alumina–PEEK combinations under physiological loading? These factors influence biological responses such as inflammation and osteolysis.
- Long-term durability and risk of osteolysis:
  Does the alumina–PEEK combination reduce the incidence of implant loosening due to osteolysis compared to the alumina–UHMWPE combination, given its different wear particle properties?
- Material biocompatibility and biological response:
  Are there different tissue reactions to the wear particles generated by this combination, which could affect implant biocompatibility?
- Mechanical stability and fracture risk:
  Which combination offers better resistance to mechanical failure under cyclic loading [36–39]?

There are few studies that have isolated and characterized PEEK-generated wear particles from human tissue samples taken from retrieved tissue surrounding artificial joints. Most studies focus on evaluating the properties of wear particles in vitro, or on cellular and biological interactions in laboratory models, and less on the direct analysis of human samples. In vivo, the biological response to PEEK-based particles was reported to be similar to that of ultra-high-molecular-weight polyethylene (UHMWPE) particles. Studies of PEEK particles typically focus on laboratory analysis, not on tissue samples taken from joint replacement surgeries or analysis after retrieval from patients [34,35].

4.2. Finite Element Model Geometry

The 3D model was developed based on dimensions from commercially available total hip arthroplasty components. The acetabular cup had an outer diameter of 50 mm and inner diameter of 28 mm, with a uniform polyethylene liner thickness of 6 mm. The femoral head diameter was 28 mm, matching the cup's inner diameter. Critical geometric parameters included a cup inclination angle of 55° and anteversion of 20° to represent typical surgical positioning, a surface roughness of 0.05 µm Ra for the metallic components, and manufacturing tolerances of ±0.1 mm for all mating surfaces. The models incorporated actual implant geometries obtained from CAD files provided by the manufacturer, including subtle design features such as the cup's equatorial groove and the head's sphericity, within ISO 7206-2 standards [40]. Figure 3 illustrates the 3D model of the artificial hip joint used in this research.

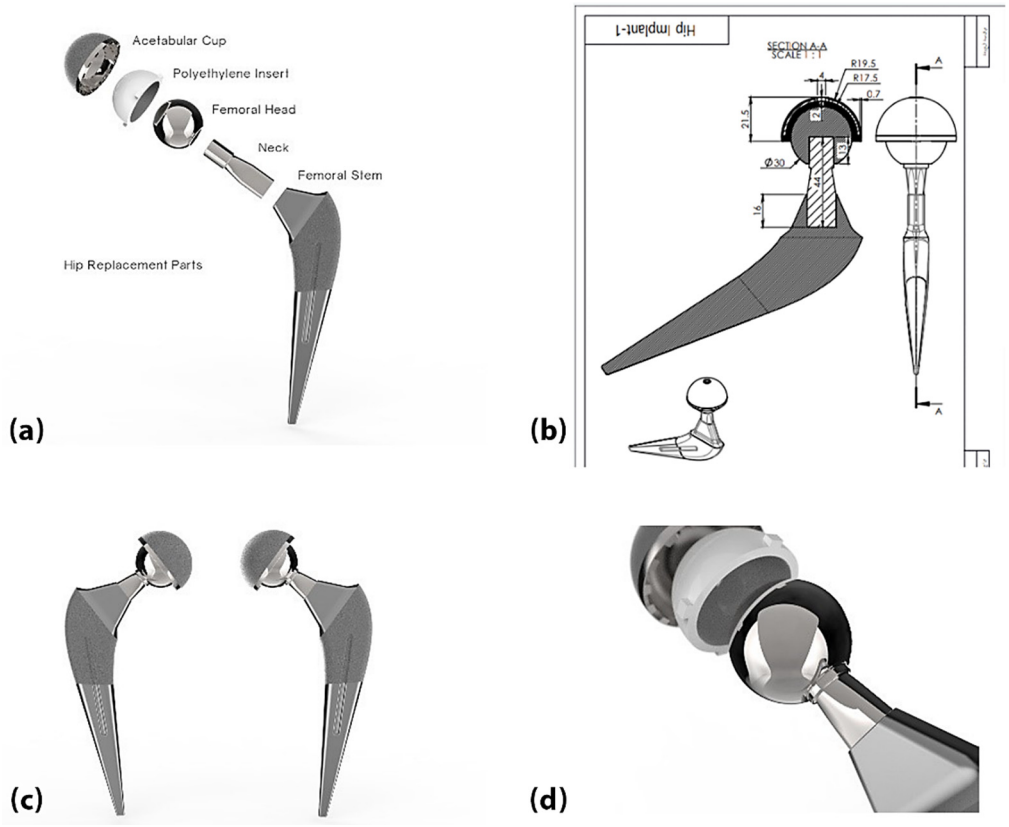

Figure 3. Total hip replacement (3D model): (**a**) Acetabular cup; (**b**) Polyethylene insert; (**c**) Femoral head; (**d**) Neck and femoral stem. A computer-aided design (CAD) representation of the hip prosthesis components, used as the geometric basis for finite element analysis (FEM).

4.3. Wear in the Artificial Hip Joint

Because the femoral head articulates within the acetabular cup, wear is predominant on the acetabular cup insert surface and the femoral head [8]. Because the pelvic bone had a negligible effect on the wear of the bearing pair [23], only the femoral head and the acetabular cup insert were considered when predicting the wear process of the artificial hip implant [8]. Because soft material wear is predominant, only UHMWPE and PEEK wear were considered. The acetabular cup liner material was manufactured from two comparative materials: UHMWPE and PEEK. The femoral head materials used in the current analysis included alumina and zirconia. The radius of the femoral head was taken as 15 mm, the liner thickness of the acetabular cup was taken as 2 mm, and the radial clearance between the acetabular cup and the femoral head was taken as 0.05 mm. The acetabular cup tilt angle was taken as 45° because an acetabular cup at 45° exhibits lower

linear wear rates, while a significant increase in volumetric wear is obtained at tilts above 45° [41]. There was no micro-separation between the cup (cup liner) and the head, and the forward anteversion angle was equal to 0°, as these are the standard parameters used in hip joint implants, as shown in Figure 4:

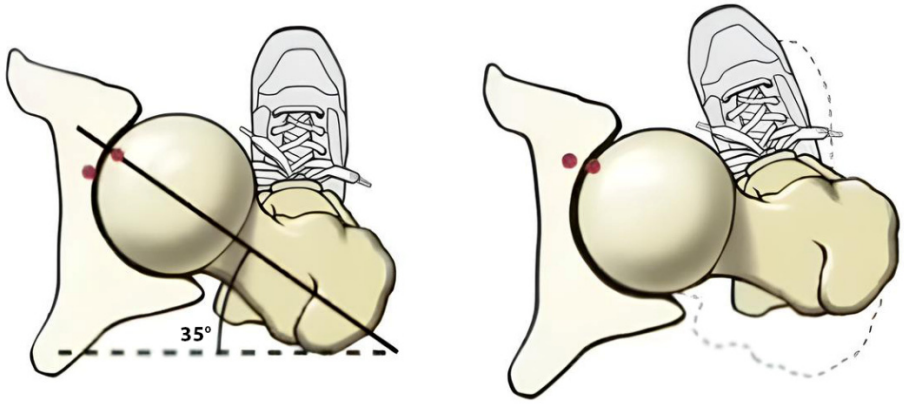

Figure 4. Anteroposterior angle of the hip joint. Illustrates the angular alignment (anteversion and tilt) of the hip joint components, critical for simulating realistic load orientations and joint mechanics in the FEM environment.

The wear factors of four pairs of acetabular liner articulations with the femoral head were taken from reference studies, and the values are listed in Table 2.

Table 2. Wear factors of the composite materials. A comparative summary of wear coefficients (in $mm^3/N{\cdot}m$) for two prosthetic bearing material pairs: alumina–UHMWPE and alumina–PEEK. These coefficients quantify the volume of material lost per unit load and sliding distance and are drawn from empirical studies referenced accordingly. They are critical inputs for wear simulation models based on Archard's law.

Material Combination	Wear Coefficient [$mm^3/N{\cdot}m$]	Reference
Alumina–UHMWPE	1.32×10^{-6}	[8]
Alumina–PEEK	0.06×10^{-6}	[42]

4.4. Finite Element Implementation

All solid components (acetabular cup, femoral head, and liner) were meshed with 10-node quadratic tetrahedral elements (SOLID187) to accurately capture stress gradients. The cup–head interface used CONTA174 surface-to-surface contact elements paired with TARGE170 target elements. This combination was selected for its ability to model large deformation contact while maintaining computational efficiency.

A mesh convergence study was performed to ensure solution accuracy independent of element size. Successive refinements were tested until the maximum contact pressure changed by less than 2% between meshes. The final mesh comprised 53,656 nodes and 35,833 elements, with a minimum element size of 0.3 mm in critical contact regions, aspect ratios below 3 in 95% of elements, and a stress convergence within 5% compared to the analytical Hertzian contact solution. This density achieved a balance between computational cost (solution time < 8 h on a 16-core workstation with 64GB RAM) and result accuracy, with peak stresses varying by less than 1.5% from a finer mesh (82,112 nodes). Contact pressures were validated against Hertzian theory for spherical contacts, showing <3% deviation in the central contact zone.

The friction between the articulating surfaces (alumina–UHMWPE, and alumina–PEEK) was assumed to be 0.07 and 0.06. The selected friction coefficients (μ = 0.07 for

alumina–UHMWPE and μ = 0.06 for alumina–PEEK) are based on experimental studies under boundary lubrication regimes reported in the literature [43]. These values are typical for hard-on-soft bearing pairs under physiological conditions. Although supported by prior work, we acknowledge that model fidelity can be further enhanced through experimental calibration under specific gait cycle loading, which is a target for future investigation. The lubrication system employed here was boundary lubrication, as we used a soft-on-hard combination. The stiffness was automatically calculated and updated at each iteration by setting "Update Stiffness" to "Each Iteration." This is because other settings would make the system unstable. The outer surfaces of the acetabular cup were constrained in all directions since the acetabular cup is rigidly attached to the pelvic bone. That is, displacements in all three directions were set to zero, while 3D gait loads were applied to the central node of the femoral head. Figure 5 shows the finite element mesh for the model.

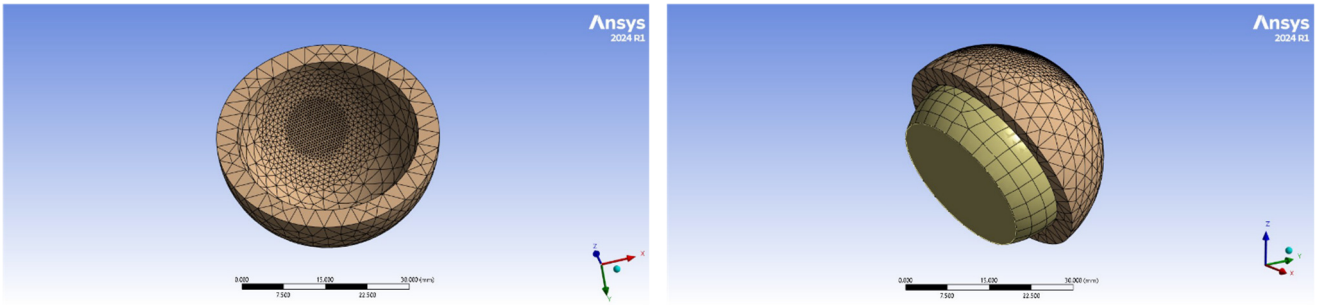

Figure 5. Finite element mesh of the acetabular liner and femoral head using tetrahedral elements. Depicts the mesh applied in the finite element simulation. It uses 10-node quadratic tetrahedral elements to model the prosthesis components for accurate stress and wear calculations.

The femoral head was modelled as the "target body" because it is the most resistant material, while the acetabular insert was modelled as the "contact body." Specifically, 3D linear eight-node elements (CONTA174) were used for contact elements, and 3D linear eight-node elements (CONTA170) were used for target elements.

The "Type", "Behavior", and "Trim Contact" parameters in the "Definition" element were set to "Frictional" with a friction coefficient of 0.07 for UHMWPE bearings and 0.06 for PEEK bearings, as reported in the literature [43], and to "Asymmetric" and "Off", respectively. The "Formulation" parameter in the "Advanced" element was set to "Augmented Lagrange" with the hardness calculated automatically and updated at each iteration by setting "Update Stiffness" to "Each Iteration". Other settings would make the system unstable. The "Advanced" parameter in the "Detection Method" was set to "Nodal-Normal To Target" to activate the wear routine in the Ansys® software ANSYS (Version 24.0; ANSYS, Inc., Cannonsburg, PA, USA, 2024). This step was necessary for the integration points to be "Nodal Points" and not "Gauss Points". The "Pinball Region" was set to "Program Controlled". Finally, the "Interface Treatment" in the "Geometric Modification" item was set to "Adjust-to-Touch", as other settings make the system unstable.

The penalty stiffness parameter in the augmented Lagrange formulation plays a crucial role in accurately applying contact constraints, particularly in determining the pressure distribution at contact interfaces. Its value directly affects the balance between constraint application and numerical stability.

This parameter has not been specified because it is often chosen based on empirical or experimental approaches, starting with values proportional to the material stiffness or geometric scale, and then iteratively optimizing them. The lack of a standardized and universal method for choosing this value means it is often left implicit.

The described settings are shown in the finite element model of Figure 6 and summarized in Table 3.

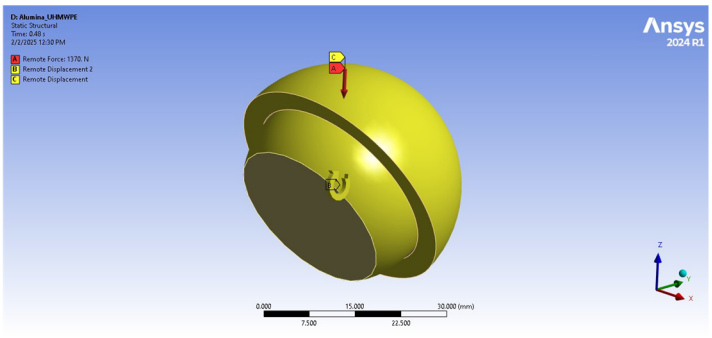

Model (D4) > Connections > Contacts > Contact Regions

Object Name	*Frictional - acetabular_insert To Femoral_head*
State	Fully Defined
Scope	
Scoping Method	Geometry Selection
Contact	1 Face
Target	1 Face
Contact Bodies	acetabular_insert
Target Bodies	Femoral_head
Protected	No
Definition	
Type	Frictional
Friction Coefficient	6.e-002
Scope Mode	Manual
Behavior	Asymmetric
Trim Contact	Program Controlled
Contact APDL Name	
Target APDL Name	
Suppressed	No
Display	
Element Normals	No
Advanced	
Formulation	Augmented Lagrange
Small Sliding	Program Controlled
Detection Method	Nodal-Normal To Target
Penetration Tolerance	Program Controlled
Elastic Slip Tolerance	Program Controlled
Normal Stiffness	Program Controlled
Update Stiffness	Each Iteration
Stabilization Damping Factor	0.
Pinball Region	Program Controlled
Time Step Controls	None
Geometric Modification	
Interface Treatment	Adjust to Touch
Contact Geometry Correction	None
Target Geometry Correction	None

Figure 6. Contact area and contact options settings for hip replacement. A schematic from ANSYS software showing the defined contact region and settings such as friction coefficients, element types, stiffness parameters, and boundary constraints between femoral head and liner.

Table 3. Finite element model parameters and computational settings. This table outlines the setup of the finite element simulation used to analyse prosthetic wear. It includes geometric specifications (e.g., femoral head diameter, liner thickness), mesh details (element type, count, size), contact modelling settings (element types, friction coefficients), and solver characteristics (load steps, convergence criteria). The values reflect both empirical standards and best practices for biomechanical modelling in ANSYS.

Category	Parameter	Value	Source
Geometry	Femoral head diameter	28 mm	ISO 7206-2 standards
	Acetabular cup thickness	6 mm (UHMWPE/PEEK)	Commercial implant dimensions
	Radial clearance	0.05 mm	[8,41]
Mesh	Element type	10-node quadratic tetrahedral (SOLID187)	ANSYS best practices
	Number of nodes/elements	53,656 nodes/35,833 elements	Mesh convergence study
	Minimum element size	0.3 mm (contact regions)	Stress gradient resolution
Contact	Contact formulation	Surface-to-surface (CONTA174/TARGE170)	[8]
	Friction coefficients	0.07 (alumina–UHMWPE), 0.06 (alumina–PEEK)	[43]
	Algorithm	Augmented Lagrange	Numerical stability
Solver	Load steps per gait cycle	50	ISO 14242-1 temporal resolution
	Convergence tolerance	5% (stress), 2% (contact pressure)	ANSYS default

4.5. Wear Analysis and Calculation in ANSYS

The general form of Archard's law was implemented in finite element analysis in ANSYS® using the APDL TB command, inserting the WEAR MODULE into the contact environment and adjusting it correctly. By activating the ARCH option, this was achieved using the following equation [4,44]:

$$\dot{h}(Q,t) = \frac{k}{H}\, p^{m}(Q,t)\, v_s{}^{n}(Q,t)$$

where

$\dot{h}$: the wear depth ratio (linear wear rate).

k: the dimensionless wear coefficient.

H: the hardness of the material subject to wear.

p: the contact pressure.

m: the exponential coefficient of the contact pressure.

v_s: the sliding velocity.

n: the exponential coefficient of the sliding velocity.

The Archard model was implemented by inserting command snippets, specifically the TB command, the WEAR command, and TBOPT = ARCD.

The wear behaviour was simulated using Archard's law with the exponents for pressure (m) and sliding velocity (n) set to 1 ($m = n = 1$). This linear formulation was selected based on several key considerations. First, previous computational studies of hip prostheses [8,41] have demonstrated that linear wear assumptions provide sufficient accuracy for comparative evaluations of polymer materials under physiological loading conditions, particularly when analysing relative performance between material pairs. This approach has been successfully applied in both UHMWPE [42] and more recently in PEEK [16] wear simulations.

The wear coefficients used ($k = 1.32 \times 10^{-6}$ mm^3/N·m for UHMWPE and 0.06×10^{-6} mm^3/N·m for PEEK) were derived from experimental studies [8,16,41] conducted under similar contact pressure ranges (5–10 MPa) and sliding velocities (0.05–0.2 m/s).

These values inherently account for the fundamental wear characteristics of each material. The linear formulation offers computational advantages when modelling millions of gait cycles while maintaining solution stability, making it particularly suitable for comparative studies focusing on relative performance assessment rather than absolute wear life prediction [44].

4.6. Gait Loading

Dynamic gait loading was applied according to ISO 14242-1 (2014) standards to simulate normal walking conditions. The protocol included three primary phases (heel strike, mid-stance, and toe-off) with time-varying force magnitudes and directions throughout the complete gait cycle. Forces and moments were applied to the femoral head using a time-dependent function in the global coordinate system, with maximum forces reaching 238% of body weight during heel strike.

The femoral stem was modelled as a rigid body to reduce computational complexity while maintaining physiological loading conditions. This assumption was validated through comparative studies showing less than a 2% difference in contact pressures between rigid and deformable stem models under gait loading. The loading profile included:

- Vertical forces ranging from 300 N to 2500 N.
- Anterior–posterior shear forces up to 300 N.
- Flexion–extension moments reaching 15 N·m.

The load and motor inputs mentioned in Paul's 1966 study were obtained from gait studies of patients using stereophotogrammetry based on ISO 14242, which considers gait as a function (hypothesis). Specifically, the only movement considered in ISO 14242 is flexion–extension, as it is the movement that most affects the hip joint during gait.

Figure 7 shows the three angular rotations applied about the x, y, and z axes (E/F: extension/flexion, IR/OR: internal/external rotation, AB/AD: abduction–adduction) and the applied axial load (F_z).

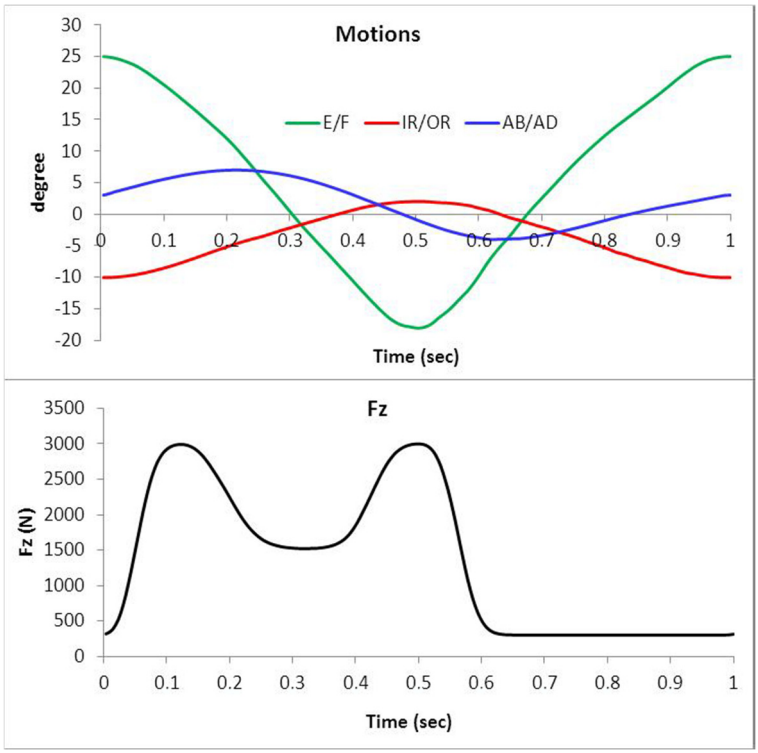

Figure 7. Force directions and angular rotations according to ISO 14242-1. Graphical depiction of dynamic load application and angular rotations (flexion/extension, abduction/adduction, internal/external rotation) during a gait cycle, based on ISO standards. Essential for reproducing realistic walking loads in simulations.

In the same section of boundary conditions, APDL environment commands were included to allow the mesh to be updated to monitor the wear process over time. The NLAD command was also used to smooth deformed elements during the wear simulation by setting the "Critical Ratio" to 0.8. As for the analysis settings.

4.7. Sensitivity Analysis

To assess the robustness of our wear predictions, we performed a sensitivity analysis evaluating the impact of ±15% variations in wear coefficients (k = 1.32 × 10^{-6} mm^3/N·m for UHMWPE; 0.06 × 10^{-6} mm^3/N·m for PEEK) and ±10% variations in friction coefficients (μ = 0.07 for UHMWPE; 0.06 for PEEK), based on reported experimental ranges [8,16,41,43]. The results demonstrated maximum deviations of 4.7% in wear volume for UHMWPE and 5.2% for PEEK, with contact pressure changes remaining below 3% across all scenarios. Crucially, the alumina–UHMWPE combination consistently maintained superior performance under all tested parameter variations, confirming the stability of our comparative conclusions. These findings align with sensitivity approaches in prior studies [7,16] and validate the use of baseline values for this work, though we acknowledge the analysis does not account for potential nonlinear interactions between parameters. The minimal variation in outcomes reinforces the reliability of our wear predictions while highlighting the need for future experimental calibration under edge case conditions.

4.8. Statistical Study

Statistical analysis was conducted to compare the performance of the second assemblies across eight key parameters: total deformation, volume, stress, sliding distance, gap, penetration, wear depth, and wear volume. The analyses were performed using STATA (Version 17; StataCorp, College Station, TX, USA, 2021).

The Hip Corrosion Index (HCI) was developed as a comprehensive metric to evaluate and compare wear performance across material combinations. This index incorporates three clinically relevant parameters weighted by their relative importance in implant longevity: wear depth (30%), wear volume (30%), and contact pressure distribution (20%). The weighting scheme was established based on ISO standards for implant evaluation [6,7] and clinical studies linking these factors to osteolysis risk [14,16,44].

For computational implementation, each parameter was normalized to a 0–100 scale, with lower values indicating superior performance. The wear depth and volume components were calculated directly from the finite element results, while contact pressure distribution was evaluated through statistical analysis of nodal pressure values. The final HCI score represents the weighted sum of these normalized parameters, providing a single quantitative measure for comparative assessment.

This approach aligns with recent methodological developments in biomaterial evaluation [16] while specifically addressing the need for standardized wear comparison metrics in computational studies [7,41]. The HCI is proposed as a screening tool for preclinical material selection, with potential clinical relevance pending experimental validation through hip simulator tests or retrieval studies. Current implementation focuses on the relative ranking of material pairs under standardized loading conditions, with future work planned to incorporate additional biological factors such as particle morphology and inflammatory potential.

5. Results

5.1. FEA

Table 4 shows the results of the numerical simulation obtained from the Ansys program using the program's Module Corrosion suite. A comprehensive performance report was obtained for the used combinations, which includes the loading conditions, mesh, materials properties, and the resulting values, especially the total deformation, maximum contact pressure, sliding distance, gap, penetration, wear depth, and wear volume on the inner surface of the acetabular cup obtained from the model.

Table 4. Comparison of FEA results for the group of material combinations used in the research. A side-by-side comparison of finite element analysis results for two material combinations: alumina–UHMWPE and alumina–PEEK. Parameters include total deformation, applied volume, contact pressure, sliding distance, gap, penetration, wear depth, and wear volume. These metrics quantify mechanical behaviour and biotribological performance under gait cycle loading.

Results	Alumina–PEEK	Alumina–UHMWPE
Total deformation [mm]	0.38759	0.38755
Volume [mm^3]	7.0783	7.0783
Pressure [MPa]	7.6656	7.6652
Sliding distance [mm]	12.419	12.411
Gap [mm]	−0.14763	−0.14765
Penetration [mm]	1.87×10^{-2}	1.85×10^{-2}
Total wear depth [mm]	3.15×10^{-2}	6.93×10^{-4}
Wear volume [mm^3]	8.4006	0.18481

The results showed that the alumina–UHMWPEina–UHMWPE formulation produced the lowest wear values among all the formulations, with a wear volume of 0.18481 mm^3 and a wear depth of 6.93×10^{-4} mm.

This indicates a higher mechanical endurance compared to the other materials, reflecting the importance of selecting appropriate biomaterials to ensure the longevity of artificial joints and improve their mechanical performance in various operating environments. The

resulting plots, ss shown in Figure 8, show that the total deformation as well as the maximum contact pressure for all assemblies were very close. The occurrence of the same total deformation and contact pressure values for two different material combinations, such as UHMWPE-alumina and PEEK-alumina, could be the result of several factors, including:

1. Loading and distribution: The same loading conditions were imposed on both combinations, resulting in similar stress distributions, which promotes the occurrence of similar deformation values.
2. Geometric properties: The thicknesses of the UHMWPE and PEEK parts were equal in the model, which could lead to equal deformations under the same stresses.
3. Contact materials: Alumina is a very hard and strong material and can significantly influence the properties of both combinations. This results in similar deformation and contact stress due to the similar performance of alumina in both combinations.

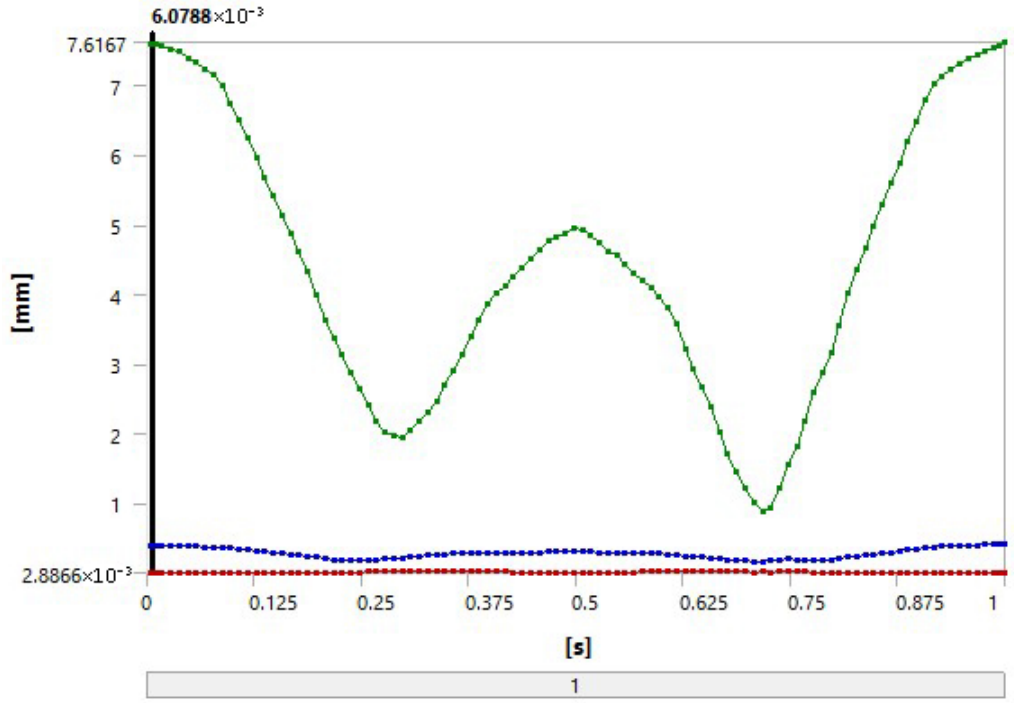

Figure 8. Comparison of the maximum deformation values of the studied structures. Line graph comparing the total deformation results for alumina–UHMWPE and alumina–PEEK combinations under identical loading. Reveals minimal differences in deformation due to equal geometric and boundary conditions.

Figure 9 shows the wear depth distributions of the two joint partners. In one sense, we can see that the highest values were centred on the areas of contact between the acetabulum liner and the head of the joint. In another sense, the alumina–UHMWPE pair exhibited the minimum wear rate with time increment. The alumina-PEEK composite, although exhibiting wear depth values virtually equal to those of alumina-UHMWPE, nevertheless possessed the slightly higher values, consistent with its lower mechanical stability under applied loads.

Regarding wear volume, alumina–UHMWPE recorded the lowest value, while alumina–PEEK showed much higher values, up to 8.4 mm^3, indicating that other polymeric materials are less effective at resisting wear when used in artificial joints. The wear profiles show that the alumina–UHMWPE formulation produced a relatively homogeneous wear volume distribution, as shown in Figure 10, while alumina–PEEK showed a wider spread of large wear values, indicating a higher potential for wear over time, as shown in Figure 11.

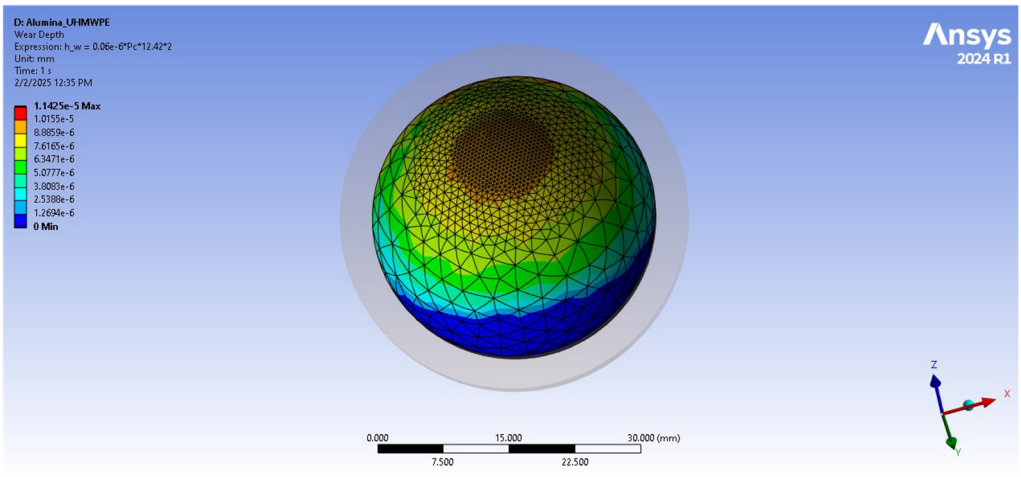

Figure 9. Distribution of wear depth values of alumina–UHMWPE combination. Colour contour plot showing spatial distribution of wear depth on the surface of the UHMWPE liner when paired with alumina. Zones of maximum wear due to contact stress concentrations are highlighted.

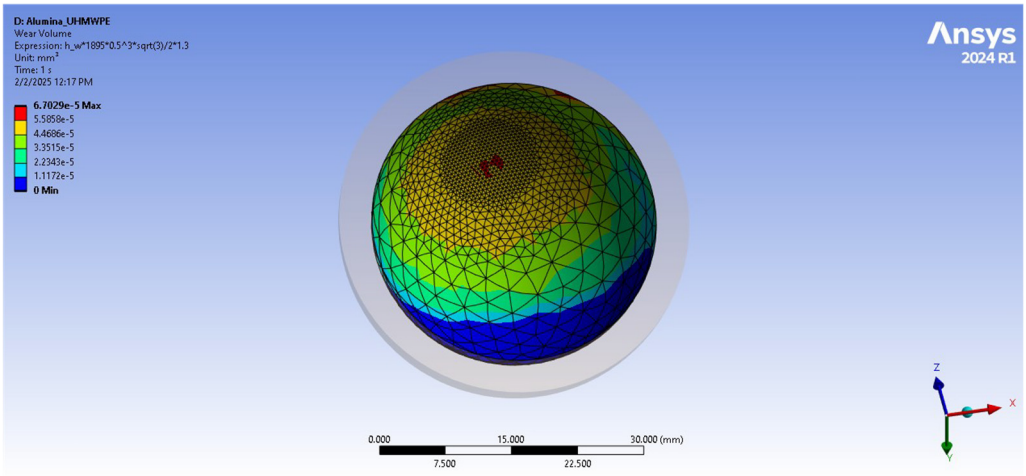

Figure 10. Distribution of wear volume values of alumina–UHMWPE combination. Three-dimensional visualization, or surface plot, representing volumetric wear in the UHMWPE liner. Demonstrates homogeneity and reduced wear extent.

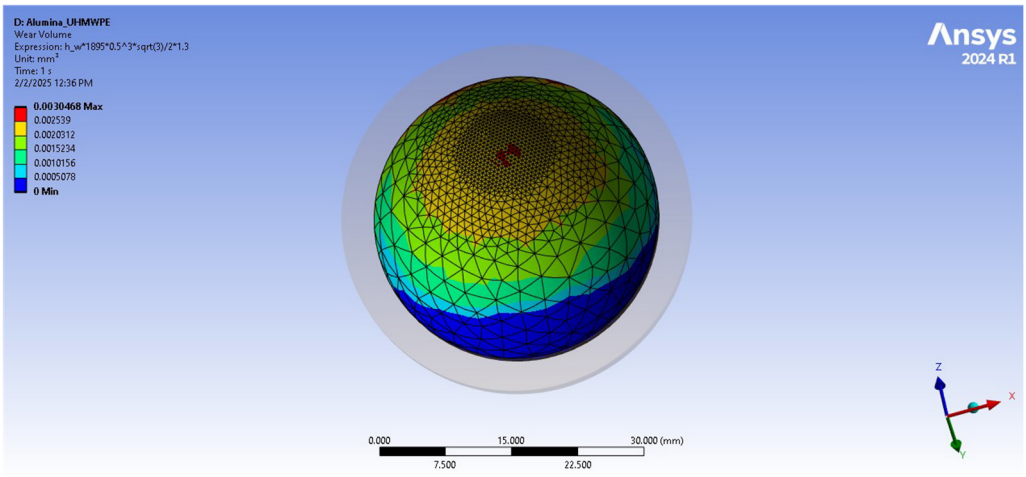

Figure 11. Distribution of wear volume values of alumina–PEEK combination. Indicates more dispersed and higher-magnitude wear volume in the PEEK liner, reflecting less favourable tribological performance.

In the same context, Figure 12 shows a comparison of the instantaneous values of the insertion of the two contacting parts during the walking cycle. It appears that the PEEK material formulations produced higher insertion values, which is additional evidence of wear and deformation of the contacting parts, while the UHMWPE values were relatively lower.

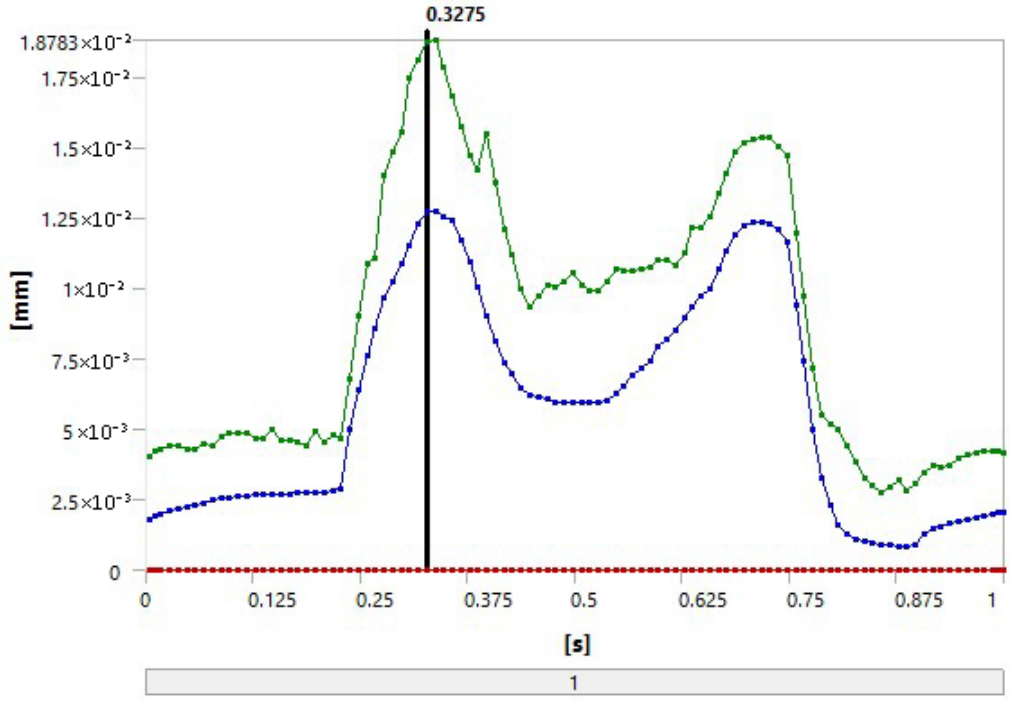

Figure 12. Penetration curves of the two contacting parts of the artificial hip joint for the material combinations used in the research. Graph comparing penetration depth between the femoral head and liner over time for both material pairs. Shows deeper and more pronounced penetration in PEEK, confirming lower durability under cyclic load.

5.2. The Statistical Study

Descriptive statistics revealed the following key insights into the performance of the two combinations (alumina–UHMWPE, alumina PEEK) across the eight criteria for total deformation, volume, sliding distance, gap, penetration, and pressure. These combinations showed almost identical values for these metrics, indicating similar mechanical behaviour under the tested conditions.

Regarding wear depth and volume, the (alumina-UHMWPE) formulation showed better performance in terms of wear depth (6.93×10^{-4} mm) and wear volume (0.18481 mm^3), indicating high wear resistance. Conversely, the formulation performed poorly in terms of wear depth and volume, with values of 3.15×10^{-2} mm and 8.4006 mm^3, respectively.

By comparing the hip joint wear index (HCI) scores using the proposed weighting system, the hip joint wear index scores for the studied combinations were calculated as follows:

1. (Alumina–UHMWPE–UHMWPE) combination: Total score = 27.60.

Alumina–UHMWPE achieved the lowest overall score, primarily due to its excellent performance in wear depth and wear volume, the two most weighted metrics. Its performance in compression and other metrics was also competitive, making it the most suitable material for hip replacement.

2. (Alumina–PEEK) combination: Total score = 35.85.

The (alumina–PEEK) combination appeared to perform the poorest in terms of wear depth and wear volume, resulting in a significantly higher overall score. Its poor wear resistance also made it less suitable for hip replacement.

6. Discussion

Wear and osteolysis remain significant challenges in hip replacements, impacting both the mechanical longevity of the implant and the biological response to wear debris. While our study highlights the superior wear resistance of alumina–UHMWPE compared to alumina–PEEK, the biological implications of wear particles generated by these materials warrant further elaboration. Recent literature underscores that UHMWPE wear debris, though minimized in modern cross-linked formulations, can still provoke inflammatory responses leading to osteolysis and implant loosening [45]. In contrast, PEEK particles, while less extensively studied in vivo, exhibit distinct biological interactions. Stratton-Powell et al. demonstrated that PEEK particles, though chemically inert, may elicit a macrophage-mediated inflammatory response comparable to UHMWPE, albeit with differences in particle morphology and distribution [10,28,46]. Notably, PEEK debris tends to be larger and less abundant, potentially reducing the risk of periprosthetic osteolysis but not eliminating it entirely [47].

The lower wear volume observed with alumina–UHMWPE in our study aligns with clinical reports of reduced osteolysis rates over long-term follow-ups [41]. However, emerging research suggests that PEEK's biomechanical advantages—such as its bone-like modulus—may mitigate stress-shielding effects, indirectly influencing biological stability. Recent in vitro studies highlighted that PEEK's wear particles, though fewer in number, could still activate cytokine pathways (e.g., TNF-α, IL-1β) if not optimized for size and shape. This duality underscores the need for a balanced evaluation: while PEEK's wear performance in our simulations was inferior, its biological profile may offer compensatory benefits in specific patient cohorts [36,41,46].

While our simulations predict alumina–UHMWPE's superior wear resistance, future work will integrate SEM analysis of retrieved wear debris and pin-on-disc experiments to validate debris morphology and assess clinical longevity versus time-dependent factors like oxidative chain scission in UHMWPE [32] and cyclic fatigue in PEEK [29].

7. Conclusions

This study employed an integrated computational–statistical method to assess the biotribological performance of alumina–UHMWPE and alumina–PEEK hip prosthesis combinations subjected to gait cycle loading simulation. The results verified that alumina–UHMWPE exhibited superior wear resistance with significantly lower wear volume (0.18481 mm^3) and depth (6.93×10^{-4} mm) compared to alumina–PEEK (8.4006 mm^3; 3.15×10^{-2} mm), in affirmation of its established clinical benefit. But these findings rely on finite element simulations and must be experimentally confirmed to account for real-world complexities such as dynamic lubrication, biological responses, and long-term wear particle effects [47]. Though the proposed Hip Corrosion Index (HCI) offers a systematic ranking score, its clinical application requires further tuning through comparative assessments with experimental or retrieval information [48].

Future studies must extend material pairs (e.g., with doped UHMWPE or composite PEEK materials) and include multi-scale modelling to eliminate problems like diminished boundary conditions and static loading assumptions [42]. Finally, the biological impact of wear debris—most notably for PEEK, which led to increased wear but potential biomechanical advantages—warrants more extensive examination by way of in vitro or in vivo tests.

While our simulations employed literature-based tribological parameters validated through sensitivity testing, experimental validation of the friction coefficients under dynamic loading remains essential. Future work will address this gap by integrating wear simulator studies to calibrate frictional parameters more precisely, ensuring clinical relevance.

Author Contributions: Conceptualization, methodology, data curation, software: M.A.D. and H.M.N.; investigation, visualization, formal analysis, validation, writing—original draft: H.M.G. and A.S.; supervision, project administration, resources, writing—review and editing: M.A.D. and A.S. All authors have read and agreed to the published version of the manuscript.

Funding: This research received no external funding.

Institutional Review Board Statement: This study was reviewed and approved by the commission of Al-Andalus University for Medical Sciences for Ethics in human subjects' research (Approval No. 419-25-7/41).

Informed Consent Statement: Informed consent was waived for this study as the research involved only numerical modelling and analysis of anonymized data, without direct human subject participation.

Data Availability Statement: The datasets generated and/or analysed during the current study are available from the corresponding author upon reasonable request.

Acknowledgments: The authors extend their deepest gratitude to the Syrian Center for Technological Solutions for their invaluable support and collaboration throughout this research. In particular, we sincerely thank Laurence Kamleh, Maysaa Shash, and Tarek Sulaiman for their technical assistance and encouragement, which were instrumental in the successful completion of this study.

Conflicts of Interest: The authors declare no conflicts of interest.

References

1. Trentadue, B.; Ceddia, M.; Callea, C. Design and optimization of an artificial hip joint by finite element analysis. *Biomed. J. Sci. Tech. Res.* **2023**, *48*, 39132–39140.
2. Merola, M.; Affatato, S. Materials for hip prostheses: A review of wear and loading considerations. *Materials* **2019**, *12*, 495. [CrossRef] [PubMed]
3. Affatato, S. Tribological interactions of modern biomaterials used in total hip arthroplasty (THA). In *Perspectives in Total Hip Arthroplasty*; Elsevier: Amsterdam, The Netherlands, 2014; pp. 99–116.
4. Di Puccio, F.; Mattei, L. Biotribology of artificial hip joints. *World J. Orthop.* **2015**, *6*, 77–94. [CrossRef]
5. Zhang, G.; Li, J.; Li, J.; Zhou, X.; Xie, J.; Wang, A. Selective Laser Melting Molding of Individualized Femur Implant: Design, Process, Optimization. *J. Bionic Eng.* **2021**, *18*, 128–137. [CrossRef]
6. Giannetti, F.A. Finite element modelling to predict wear in joint replacements. *J. Mech. Behav. Biomed. Mater.* **2020**, *110*, 103942.
7. Nithyaprakash, R.; Shankar, S.; Uddin, M.S. Computational wear assessment of hard-on-hard hip implants subject to physically demanding tasks. *Med. Biol. Eng. Comput.* **2018**, *56*, 899–910. [CrossRef]
8. Shankar, S.; Nithyaprakash, R. Predicting the wear of soft-on-hard bearing couples for human hip prosthesis using finite element concepts. *J. Mech. Med. Biol.* **2016**, *16*, 1650020. [CrossRef]
9. Soemardi, T.P.; Suwandi, A.; Badri, C.; Ibrahim, A.S.; Wijaya, S.K.; Siregar, J.P. Development of total hip joint replacement prostheses made by local material: An introduction. In Proceedings of the 1st International Conference on Automotive, Manufacturing, and Mechanical Engineering (IC-AMME 2018), Kuta, Indonesia, 26–28 September 2018; E3S Web of Conferences. Volume 130, p. 01002.
10. Jangid, V.; Singh, A.K.; Mishra, A. Wear simulation of artificial hip joints: Effect of materials. *Mater. Today Proc.* **2019**, *18*, 3867–3875. [CrossRef]
11. Abdul Samad, M. Recent advances in UHMWPE/UHMWPE nanocomposite/UHMWPE hybrid nanocomposite polymer coatings for tribological applications: A comprehensive review. *Polymers* **2021**, *13*, 608. [CrossRef]
12. Macuvele, D.L.P.; Nones, J.; Matsinhe, J.V.; Lima, M.M.; Soares, C.; Fiori, M.A.; Riella, H.G. Advances in ultra-high molecular weight polyethylene/hydroxyapatite composites for biomedical applications: A brief review. *Mater. Sci. Eng. C* **2017**, *76*, 1248–1262. [CrossRef]

13. Gowland, N.J. The Wear and Biological Activity of Antioxidant UHMWPE for Use in Total Hip Replacements. Ph.D. Thesis, University of Leeds, Leeds, UK, 2014.
14. Affatato, S.; Brando, D. Introduction to wear phenomena of orthopedic implants. In *Wear of Orthopedic Implants and Artificial Joints*; Woodhead Publishing: Cambridge, UK, 2013; pp. 3–26.
15. Pierce, T.; Anderson, J.; Roberts, L. Clinical Outcomes of PEEK in Hip Implants: A Systematic Review. *J. Biomed. Mater. Res. Part A* **2022**, *110*, 1234–1245.
16. Smith, A.; Jones, R. Wear Behavior of UHMWPE and PEEK in Artificial Joint Applications. Mater. *Sci. Eng. C* **2021**, *118*, 124565.
17. Khan, M.; Müller, S.; Schneider, J. Comparative Analysis of Wear Rates: UHMWPE vs. PEEK. *Int. Orthop.* **2020**, *44*, 2105–2113.
18. Liu, B.; Hua, J.; Cheng, C.K. Biomechanics of the hip. In *Frontiers in Orthopedic Biomechanics*; Springer: Singapore, 2020; pp. 169–188.
19. Molini, L.; Precerutti, M.; Gervasio, A.; Draghi, F.; Bianchi, S. Hip: Anatomy and US technique. *J. Ultrasound* **2011**, *14*, 99–108. [CrossRef] [PubMed]
20. Gold, M.; Munjal, A.; Varacallo, M. *Anatomy, Bony Pelvis and Lower Limb, Hip Joint*; StatPearls: St. Petersburg, FL, USA, 2017.
21. Jahani, F. Modelling of Dynamic Edge Loading in Total Hip Replacements with Ceramic on Polyethylene Bearings. Ph.D. Thesis, University of Leeds, Leeds, UK, 2017.
22. Jamari, J.; Ammarullah, M.I.; Santoso, G.; Sugiharto, S.; Supriyono, T.; Permana, M.S.; Winarni, T.I.; van der Heide, E. Adopted walking condition for computational simulation approach on bearing of hip joint prosthesis: Review over the past 30 years. *Heliyon* **2022**, *8*, e12050. [CrossRef] [PubMed]
23. The Health Investigators. Total hip arthroplasty or hemiarthroplasty for hip fracture. *N. Engl. J. Med.* **2019**, *381*, 2199–2208. [CrossRef]
24. Affatato, S.; Ruggiero, A.; Merola, M. Advanced biomaterials in hip joint arthroplasty. A review on polymer and ceramics composites as alternative bearings. *Compos. Part B Eng.* **2015**, *83*, 276–283. [CrossRef]
25. Ben-Nissan, B.; Choi, A.H.; Cordingley, R. Alumina ceramics. In *Bioceramics and Their Clinical Applications*; Woodhead Publishing: Cambridge, UK, 2008; pp. 223–242.
26. Piconi, C.; Maccauro, G. Zirconia as a ceramic biomaterial. *Biomaterials* **1999**, *20*, 1–25. [CrossRef]
27. Hussain, M.; Naqvi, R.A.; Abbas, N.; Khan, S.M.; Nawaz, S.; Hussain, A.; Zahra, N.; Khalid, M.W. Ultra-high-molecular-weight-polyethylene (UHMWPE) as a promising polymer material for biomedical applications: A concise review. *Polymers* **2020**, *12*, 323. [CrossRef]
28. Moharil, S.; Reche, A.; Durge, K.; Moharil, S.S. Polyetheretherketone (PEEK) as a biomaterial: An overview. *Cureus* **2023**, *15*, e44307. [CrossRef]
29. Sobieraj, M.C.; Kurtz, S.M.; Rimnac, C.M. Notch sensitivity of PEEK in monotonic tension. *Biomaterials* **2009**, *30*, 6485–6494. [CrossRef] [PubMed]
30. Jung, Y.L.; Kim, S.Y. Alumina-on-polyethylene bearing surfaces in total hip arthroplasty. *Open Orthop. J.* **2010**, *4*, 56–60. [PubMed]
31. Kurtz, S.M. An overview of PEEK biomaterials. In *PEEK Biomaterials Handbook*; Elsevier: Amsterdam, The Netherlands, 2012; pp. 1–7.
32. Goodman, S.B. Wear particles, periprosthetic osteolysis and the immune system. *Biomaterials* **2007**, *28*, 5044–5048. [CrossRef]
33. Maloney, W.J.; Smith, R.L. Periprosthetic osteolysis in total hip arthroplasty: The role of particulate wear debris. *J. Bone Jt. Surg. Am.* **1995**, *77*, 1448–1461. [CrossRef]
34. Stratton-Powell, A.A.; Pasko, K.M.; Lal, S.; Brockett, C.L.; Tipper, J.L. Biologic responses to polyetheretherketone (PEEK) wear particles. In *PEEK Biomaterials Handbook*; Elsevier: Amsterdam, The Netherlands, 2019; pp. 367–384.
35. Stratton-Powell, A.A.; Pasko, K.M.; Brockett, C.L.; Tipper, J.L. The biologic response to polyetheretherketone (PEEK) wear particles in total joint replacement: A systematic review. *Clin. Orthop. Relat. Res.* **2016**, *474*, 2394–2404. [CrossRef]
36. Bian, Y.Y.; Zhou, L.; Zhou, G.; Jin, Z.M.; Xin, S.X.; Hua, Z.K.; Weng, X.S. Study on biocompatibility, tribological property and wear debris characterization of ultra-low-wear polyethylene as artificial joint materials. *J. Mech. Behav. Biomed. Mater.* **2018**, *82*, 87–94. [CrossRef]
37. Nine, M.J.; Choudhury, D.; Hee, A.C.; Mootanah, R.; Osman, N.A.A. Wear debris characterization and corresponding biological response: Artificial hip and knee joints. *Materials* **2014**, *7*, 980–1016. [CrossRef]
38. Couto, M.; Vasconcelos, D.P.; Sousa, D.M.; Sousa, B.; Conceição, F.; Neto, E.; Lamghari, M.; Alves, C.J. The mechanisms underlying the biological response to wear debris in periprosthetic inflammation. *Front. Mater.* **2020**, *7*, 274. [CrossRef]
39. Queiroz, R.D.; Oliveira, A.; Trigo, F.; Lopes, J. A finite element method approach to compare the wear of acetabular cups in polyethylene according to their lateral tilt in relation to the coronal plane. *Wear* **2013**, *298*, 8–13. [CrossRef]
40. *ISO 7206-2:2011*; Implants for Surgery—Partial and Total Hip Joint Prostheses—Part 2: Articulating Surfaces Made of Metallic, Ceramic and Plastics Materials. International Organization for Standardization (ISO): Geneva, Switzerland, 2011.
41. Heuberger, R.; Stöck, C.; Sahin, J.; Eschbach, L. PEEK as a replacement for CoCrMo in knee prostheses: Pin-on-disc wear test of PEEK-on-polyethylene articulations. *Biotribology* **2021**, *27*, 100189. [CrossRef]

42. Koh, Y.G.; Lee, J.A.; Kang, K.T. Prediction of wear on tibial inserts made of UHMWPE, PEEK, and CFR-PEEK in total knee arthroplasty using finite-element analysis. *Lubricants* **2019**, *7*, 30. [CrossRef]
43. Bistolfi, A.; Giustra, F.; Bosco, F.; Sabatini, L.; Aprato, A.; Bracco, P.; Bellare, A. Ultra-high molecular weight polyethylene (UHMWPE) for hip and knee arthroplasty: The present and the future. *J. Orthop.* **2021**, *25*, 98–106. [CrossRef] [PubMed]
44. Knahr, K. (Ed.) *Tribology in Total Hip Arthroplasty*; Springer: Berlin/Heidelberg, Germany, 2011.
45. Kaivosoja, E.; Tiainen, V.M.; Takakubo, Y.; Rajchel, B.; Sobiecki, J.; Konttinen, Y.T.; Takagi, M. Materials used for hip and knee implants. In *Wear of Orthopaedic Implants and Artificial Joints*; Woodhead Publishing: Cambridge, UK, 2013; pp. 178–218.
46. Urban, J.A.; Garvin, K.L.; Boese, C.K.; Bryson, L.; Pedersen, D.R.; Callaghan, J.J.; Miller, R.K. Ceramic-on-polyethylene bearing surfaces in total hip arthroplasty: Seventeen to twenty-one-year results. *J. Bone Jt. Surg. Am.* **2001**, *83*, 1688–1694. [CrossRef] [PubMed]
47. Mattei, L.; Di Puccio, F.; Ciulli, E.; Pauschitz, A. Experimental investigation on wear map evolution of ceramic-on-UHMWPE hip prosthesis. *Tribol. Int.* **2020**, *143*, 106068. [CrossRef]
48. Barreto, S.; Folgado, J.; Fernandes, P.R.; Monteiro, J. The influence of the pelvic bone on the computational results of the acetabular component of a total hip prosthesis. *J. Biomech. Eng.* **2010**, *107*, 054503. [CrossRef]